RESEARCH ARTICLE

Key Points:
- Since the 1990s, parts of the Yukon coast are in a phase of enhanced shoreline retreat
- Gravel features grew in areal extent since the 1950s and were largest in the latest measurements in 2011
- Extensive parts of the coast are prone to flooding due to low backshore elevation

Correspondence to:
A. M. Irrgang,
anna.irrgang@awi.de

Variability in Rates of Coastal Change Along the Yukon Coast, 1951 to 2015

Anna M. Irrgang[1,2] iD, **Hugues Lantuit**[1,2] iD, **Gavin K. Manson**[3], **Frank Günther**[1] iD, **Guido Grosse**[1,2] iD, and **Pier Paul Overduin**[1] iD

[1]Department of Periglacial Research, Alfred Wegener Institute Helmholtz Centre for Polar and Marine Research, Potsdam, Germany, [2]Institute of Earth and Environmental Science, University of Potsdam, Postdam, Germany, [3]Geological Survey of Canada-Atlantic, Dartmouth, Canada

Abstract To better understand the reaction of Arctic coasts to increasing environmental pressure, coastal changes along a 210-km length of the Yukon Territory coast in north-west Canada were investigated. Shoreline positions were acquired from aerial and satellite images between 1951 and 2011. Shoreline change rates were calculated for multiple time periods along the entire coast and at six key sites. Additionally, Differential Global Positioning System (DGPS) measurements of shoreline positions from seven field sites were used to analyze coastal dynamics from 1991 to 2015 at higher spatial resolution. The whole coast has a consistent, spatially averaged mean rate of shoreline change of 0.7 ± 0.2 m/a with a general trend of decreasing erosion from west to east. Additional data from six key sites shows that the mean shoreline change rate decreased from −1.3 ± 0.8 (1950s–1970s) to −0.5 ± 0.6 m/a (1970s–1990s). This was followed by a significant increase in shoreline change to −1.3 ± 0.3 m/a in the 1990s to 2011. This increase is confirmed by DGPS measurements that indicate increased erosion rates at local rates up to −8.9 m/a since 2006. Ground surveys and observations with remote sensing data indicate that the current rate of shoreline retreat along some parts of the Yukon coast is higher than at any time before in the 64-year-long observation record. Enhanced availability of material in turn might favor the buildup of gravel features, which have been growing in extent throughout the last six decades.

Plain Language Summary The Arctic is warming, but the impacts on its coasts are not well documented. To better understand the reaction of Arctic coasts to increasing environmental pressure, shoreline position changes along a 210-km length of the Yukon Territory coast in northwest Canada were investigated for the time period from 1951 to 2015. Shoreline positions were extracted from historical aerial images from the 1950s, 1970s, and 1990s and from satellite images from 2011. Additionally, measurements of shoreline positions from field sites were used to analyze coastal dynamics from 1991 to 2015. The mean shoreline change rate was −1.3 m/a between the 1950s and 1970s and followed by a decrease to −0.5 m/a between the 1970s to 1990s. This was followed by a significant increase in mean shoreline change rates again to −1.3 m/a in the 1990s to 2011 time period. This acceleration in erosion is confirmed by field measurements that indicate increased erosion rates at high local rates up to −8.9 m/a since 2006. Enhanced coastal erosion might, in turn, favor the buildup of gravel features, which have been growing in extent throughout the last six decades.

1. Introduction

Permafrost coasts are highly dynamic landscapes in the Arctic. Approximately 65% of all Arctic coasts are unlithified but bonded by permafrost, which is defined as ground that stays below 0 °C for at least two consecutive years (Harris et al., 1988; Lantuit et al., 2012). Upon thaw, many of these coasts are affected by high erosion rates (Günther et al., 2015; Jones et al., 2013; Lantuit et al., 2012). Erosion can have large impacts on the ecological and socioeconomical dimension of coastal systems. Since large quantities of organic carbon are stored in permafrost, released fluxes from coastal erosion could form a significant contribution to the Arctic carbon cycle (Callaghan et al., 2011; Fritz et al., 2017; Hugelius et al., 2013; McGuire et al., 1995; Tanski et al., 2017; Vonk et al., 2012; Zhang & Chen, 2005). Coastal erosion is also threatening infrastructure, settlements, and archeological sites along many Arctic coasts (Forbes, 2011; Radosavljevic et al., 2015; Ogorodov et al., 2016; O'Rourke, 2017).

In the Arctic, air temperatures are expected to increase by 4 to 12 °C (RCP 8.5) by 2081–2100 relative to 1986–2005 (Intergovernmental Panel on Climate Change, 2013). Increasing air temperatures lead to

higher permafrost and water temperatures (Arctic Monitoring and Assessment Programme, 2011; Overland et al., 2015; Proshutinsky et al., 2015; Smith et al., 2010), decreasing sea ice extent and thickness (Serreze et al., 2009; Stroeve et al., 2007, 2011, 2014) and longer open water seasons (Markus et al., 2009; Stroeve et al., 2014), higher frequency of more severe storms (Atkinson, 2005; Manson et al., 2005), rising sea level (Manson & Solomon, 2007), and deeper thawing depths of soils (Grosse et al., 2016; Hinzman et al., 2005). All these changes have the potential to enhance coastal erosion, especially along coasts with high ground ice contents (Aré, 1988; Dallimore et al., 1996; Günther et al., 2015; Kizyakov et al., 2013; Lantuit & Pollard, 2008). Yet the rate at which Arctic coasts are responding to these changes is not well known, since baseline shoreline change data sets covering multiple time periods are very scarce.

Accelerated shoreline retreat has been reported from several locations along Arctic coasts, but no Arctic-wide acceleration in shoreline retreat has yet been substantiated, likely because of the lack of suitable data and the scarce coverage of Arctic coastal change studies (Overduin et al., 2014). High coastal erosion rates have been described along the Siberian coast, with acceleration of coastal erosion being observed in various studies with rates up to -17 m/a along very exposed sites, like the northern tip of Muostakh Island (Günther et al., 2013, 2015; Lantuit et al., 2011; Maslakov & Kraev, 2016; Vasiliev et al., 2005). Along the Alaskan Beaufort coast, mean shoreline change occurs at a rate of -1.4 ± 0.3 m/a (1940s–2000s), and maximum rates of up to -19 m/a are being measured in the area of Drew Point and Point Barrow for subdecadal time periods (Barnhart, Anderson, et al., 2014; Brown et al., 2003; Gibbs & Richmond, 2015; Jones et al., 2008, Jones, Arp, Beck, et al., 2009, Jones, Arp, Jorgenson, et al., 2009; Mars & Houseknecht, 2007; Ping et al., 2011; Reimnitz et al., 1985; Tweedie et al., 2012). However, despite the fact that the Yukon coast is one of the most ice-rich and fastest eroding coasts in the Arctic (Lantuit et al., 2012), little is known about the spatial and temporal variability over timescales of decades and the spatial scale of the entire coast. The only study systematically investigating the whole Yukon coast by means of aerial imagery analyses from the 1950s and 1970s was published in 1985 and reported average retreat rates of -0.5 m/a with local rates up to -5.3 m/a (Harper et al., 1985). Further studies have concentrated on shorter parts of the Yukon coast (Forbes, 1997; Konopczak et al., 2014; Lantuit & Pollard, 2008; McDonald & Lewis, 1973; Radosavljevic et al., 2015) or on much shorter timescales (Obu et al., 2017). These studies reported mean shoreline change rates of -0.45 to -3.0 m/a, which corresponds well with shoreline change rates published by Harper et al. (1985). Since most of these studies published rates of shoreline change for one to two time periods, no conclusive insight into possible change in trends in shoreline change rates could be gained so far.

In this paper, the previous studies are complemented and significantly expanded by (1) quantifying shoreline position changes along 210 km of the Yukon coast over a 64-year period (1951–2015) and (2) investigating the temporal and spatial variability of these shoreline changes.

2. Study Area

The Yukon coast is the northern limit of the Yukon Coastal Plain, which is the emergent part of the Beaufort continental shelf (Figure 1). The Yukon Coastal Plain is 10 to 40 km wide and extends from the Alaskan border to the Mackenzie delta (Rampton, 1982). The Yukon coast region was partially glaciated by an extension tongue of the Laurentide Ice Sheet flowing from the southeast during the Buckland Stage of the Wisconsin glaciation about 40 ka BP (Rampton, 1982). During glacial advance, the ice sheet deformed sediments and left extensive morainic deposits behind after retreat. The progression stopped at what is today the fan of the Firth River. The region is therefore characterized by two distinct physiographic areas located on either side of this glacial limit (Fritz et al., 2012; Rampton, 1982; Figure 1).

The coast which remained unglaciated during the last ice age west of the Firth River delta is characterized by a gently sloping backshore composed of fine-grained lacustrine and alluvial sediments (Rampton, 1982). Coastal cliffs are 6 m high near the Canada-U.S. American border and decrease in height to 3 m toward Komakuk Beach. Ground ice volumes of up to 66% (Couture, 2010) between Komakuk Beach and the Canada-U.S. American border result in thermo-abrasion and thermo-denudation processes that alter the landscape, for example, by active layer detachments, or block failures (Konopczak et al., 2014). The river deltas of the Malcom and Firth River are fronted by a 30.5-km-long system of barrier spits and barrier islands termed Nunaluk Spit, which protects the delta coast (Figure 1).
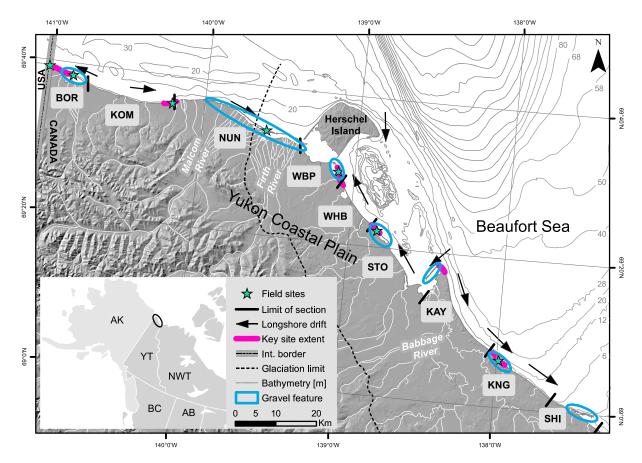
Figure 1. Yukon coast with subregions identified: (1) BOR (Border, including Clarence Lagoon), (2) KOM (Komakuk Beach), (3) NUN (Nunaluk Spit), (4) WBP (Workboat Passage, including Catton Point), (5) WHB (Whale Bay), (6) STO (Stokes Point), (7) KAY (Kay Point), (8) KNG (King Point), and (9) SHI (Shingle Point). The stars mark the field sites, along which GPS measurements were taken. These are from west to east: BORs, CLAs, KOMs, CATs, NUNs, STOs, and KNGs. The purple bars mark the key site extents. These key sites are additionally covered by aerial images from the 1990s. Blue circles indicate the seven main gravel features along the coast, which were assessed to analyze land change dynamics. They are from west to east: Clarence Lagoon, Nunaluk Spit, Catton Point Spit, Stokes Point Lagoon, Kay Point Spit, King Point Lagoon, and Shingle Point Spit. Longshore drift information was obtained from the Environmental Atlas of the Beaufort Coastlines 2016. Bathymetric contours information is based on Canadian Hydrographic Survey Navigational Charts and was improved by local surveys performed in the 1980s (Thompson, 1994). Basemap: 30 m Yukon Digital Elevation Model, interpolated from the digital 1:50,000 Canadian Topographic Database (Yukon Department of Environment, 2016).

The formerly glaciated part of the coast, east of the Malcom river delta, is composed of fine-grained lacustrine and outwash plains, as well as rolling moraines that contain coarse grained tills (Bouchard, 1974; Rampton, 1982). The morphology of this formerly glaciated section of coast is much more diverse than to the west. From the Workboat Passage to the Babbage River delta, cliff heights vary between 2- and 3-m (toward the west) to 15-m-high ice-rich cliffs (toward the east). From Kay Point to Shingle Point, the coast rises up to 60 m high and is mainly characterized by steep cliffs made of till deposits, often with very high ground ice contents up to 74% (Couture, 2010) including massive ground ice beds (Harry et al., 1988). Processes such as retrogressive thaw slumping and cliff face gullying are characteristic for this region, as well as block failure along the coast as a consequence of thermal abrasion at the cliff toe (Wolfe et al., 2001).

The Canadian Beaufort shelf fronting the Yukon Coastal Plain is 40 to 150 km wide and is gently sloping toward the shelf break located approximately at the 80-m isobath (Hill et al., 1991). The period of time when sea ice is absent and liquid water and waves affect the shoreface is limited to about 3.5 months from late June to early October (Galley et al., 2016). Observations show that this period elongates throughout the satellite data record, which started in 1979. The length of the season when sea ice is absent along the Beaufort coast extended by 9 days per decade from 1979 to 2013 (Stroeve et al., 2014). Relative sea-level rise in this region is on average approximately 2 mm/a (James et al., 2014). Astronomical tides are semidiurnal and in the micro-tidal (0.3 to 0.5 m) range (Héquette et al., 1995). However, storm surges can raise water levels up to 3 m and

Table 1
Overview Over Data Sets Used for Shoreline Change Detection at Different Spatial and Temporal Scales

Name	Scale	Data sets	Resolution (m)	Approximate total length (km)	Approximate min. to max. length of single site (km)
Whole coast	Regional	Remotely sensed images from the 1950s, 1970s, and 2011	0.5–3.5	210.0	
Subregions	Subregional	Remotely sensed images from the 1950s, 1970s, and 2011	0.5–3.5	210.0	11.7–33.6
Key sites	Subregional	Remotely sensed images from the 1950s, 1970s, 1990s, and 2011	0.5–3.5	27.0	3.0–7.0
Gravel features	Subregional	Remotely sensed images from the 1950s, 1970s, and 2011	0.5–3.5	59.5	3.1–30.5
Field sites	Local	GPS data, several years between 1991 and 2015 (Table 4)	0.05–0.10	2.5	0.1–1.7

can cause large-scale flooding (Harper et al., 1988; Reimnitz & Maurer, 1979). The prevailing wind directions are from the southeast and northwest, though most storms come from the northwest (Hill et al., 1991; Hudak & Young, 2002). Storms from the northeast generate negative surges and are thus less effective in eroding the coast (Harper & Penland, 1982; Henry, 1975). Storm occurrences usually peak within the last month before sea ice freeze-up in October (Atkinson, 2005; Hudak & Young, 2002).

The mean annual temperature for Komakuk Beach is −11.0 °C, with a July maximum of 7.8 °C (1971–2000; Environment Canada, 2016). The Yukon Coastal Plain is underlain by continuous permafrost except beneath large thermokarst lakes and riverbeds (Rampton, 1982). Permafrost temperature has been warming at the top of permafrost at Herschel Island by up to 2.6 °C since 1905 (Burn & Zhang, 2009). This increase is linked to a warming of air temperatures, which are 2.8 °C higher than the ones of the early twentieth century (Richter-Menge & Mathis, 2016).

2.1. Data and Methods

In order to understand how the shoreline changed along a large portion of the Yukon coast, a 210-km length of coast from the Canada-U.S. American border in the west to Shingle Point in the east was investigated on different spatial and temporal scales using remotely sensed images and field survey data (Table 1).

2.2. Remote Sensing Data

A combination of aerial images and satellite images was used to map shoreline positions. A series of scanned aerial monochrome (i.e., black and white) images were obtained from the Canadian National Air Photo Library (Natural Resources Canada (NRCan), 2016a) for the 1950s (i.e., 1951, 1952, 1953, and 1954), the 1970s (i.e., 1972 and 1976), and the 1990s (i.e., 1992, 1994, and 1996). No single year of imagery in the 1950s or 1970s had complete coverage of the study area. Thus, images from multiple years within each decade were combined to produce a single shoreline data set for each of those decades. Additionally, seven short shoreline sections (key sites) were covered by aerial images in the 1990s, together covering a coastal length of 27 km (Figure 1). The coverage by aerial images in the 1990s was mostly determined by where field sites were situated at that time (Figure 1, section 2.3). The 2011 shoreline position was mapped using satellite images (Digital Globe, 2014, 2016). Subsequently, all aerial images from 1951, 1952, 1953, and 1954 will be referred to as the 1950s aerial image series. The aerial images from 1972 and 1976 will be referred to as the 1970s aerial image series, and the ones from 1992, 1994, and 1996 as the 1990s aerial image series.

2.2.1. Geo-Coding

Orthorectification of all aerial images was performed by geocoding all images to the 2011 satellite images using PCI Geomatic's Geomatica Orthoengine© software (2014). The absolute geolocation accuracy for GeoEye-1 and WorldView-2 images is better than 5 and 3.5 m, respectively (Digital Globe, 2014, 2016). The PCI Geomatic's Geomatica Orthoengine© software accounts for camera tilt, lens distortion, radial distortion, Earth curvature, and refraction when orthorectifying aerial images. Digital elevation data sets were used to reduce displacement caused by terrain relief. These included the Yukon Digital Elevation Model (30.0-m ground resolution; Environment Yukon, 2016), airborne LiDAR (light detection and ranging) elevation data (1.0-m ground resolution and vertical accuracy of 0.15 ± 0.1 m) (Kohnert et al., 2014; Obu et al., 2016, 2017), and the TanDEM-X intermediate digital elevation model (12.0-m ground resolution; Huber et al., 2012). Each image was orthorectified to the average height of the digitized shoreline position. Therefore, the elevation data with the highest resolution and best coverage were used for each aerial image. Aerial images from the 1950s and 1970s have a ground resolution of 3.5 and 3.0 m, respectively.

Table 2
Metadata and Accuracy for Remotely Sensed Images

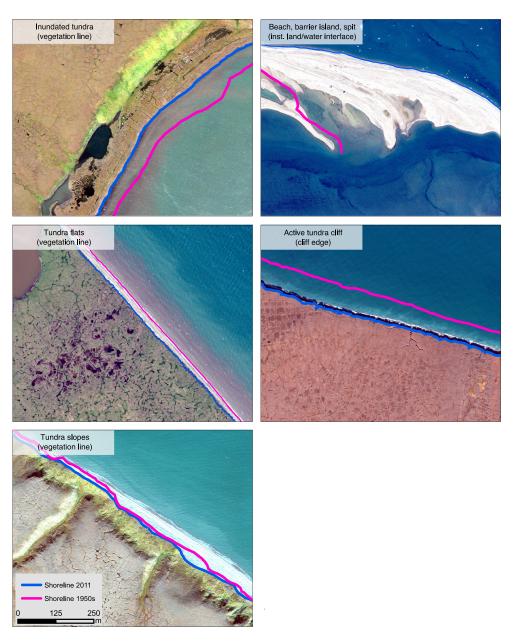| Date	Number of images	Type of image	Scale 1 to	Ground resolution (E_{GRa}; m)	GCPs (TPs)	RMS (m)	LOA (m)	U (m)
18 Jul 2011	1	GeoEye-1 (multispectral pansharpened)	/	0.4	Base image	/	2	2.06
20 Jul 2011	1							
31 Aug 2011	1							
13 Sep 2011	1							
31 Aug 2011	1	WordView-2 (multispectral pansharpened)	/	0.5	Base image	/	2	2.06
13 Sep 2011	1							
25 Jul 1996	11	Monochrome air photos	6,000	0.3	520 (159)	1.00 to 2.82	2	2.26 to 3.47
13 Jul 1994	11							
08 Jun 1992	21							
07 Jul 1976	1	Monochrome air photos	60,000	3.0	261 (56)	7.91	4	11.02
08 Jul 1972	3							
09 Jul 1972	8							
31 Jul 1972	3							
14 Aug 1972	5							
22 Aug 1954	8	Monochrome air photos	70,000	3.5	202 (80)	4.42	7	9.55
27 Jul 1953	3							
20 Jul 1952	3							
14 Jul 1951	3							

Note. E_{GR} is ground resolution, GCP stands for ground control point, TP for tie point, RMS for the average root mean square error of all Orthoengine© projects for one decade, LOA for loss of accuracy, and U for shoreline uncertainty. The supporting information Figures S1, S2, and S3 provide additional information (year, roll number, and picture number), as well as the footprint for each aerial image.
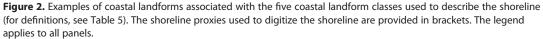
This means that the smallest distinguishable objects are 3.5 (1950s) or 3.0 m (1970s) apart. The aerial images from the 1950s were taken in four consecutive years (i.e., 1951, 1952, 1953, and 1954; supporting information Figure S1). The aerial images from the 1970s were all taken in 1972, except for the one in 1976 (supporting information Figure S2). Assuming that landscape changes that occurred between the overflights from 1951 until 1954 and from 1972 and 1976 are within the range of the ground resolution, aerial images from the 1950s and 1970s were processed together as a combined decadal data set, respectively. This means that all images from the 1950s and from the 1970s were combined and processed together in one PCI project, resulting in one mosaic data set for the 1950s and one for the 1970s. The 1990s were treated differently. Aerial images from different years were not combined, since the images covered six separate locations, instead of one coherent area along the whole coast (supporting information Figure S3). Thus, six mosaic data sets were created, each of them covering one key site and combining aerial images from 1 year. A total number of 520, 261, and 202 ground control points were used to orthorectify the 1950s, 1970s and 1990s images to the 2011 satellite images, respectively. The root mean square (RMS) positional errors for the orthorectified aerial images were 4.42 and 7.91 m for the 1950s and the 1970s PCI project, respectively (Table 2). For the 1990s, project RMS values were between 1.00 and 2.82 m (Table 2). The overall PCI project RMS values provide information about the mean offset of all pictures in a project. However, the validity of the PCI project RMS for each aerial image is limited.

2.2.2. Shoreline Digitalization

The shoreline was digitized manually on screen at a consistent zoom level equivalent to a scale of 1:1,000. Because of the wide range of landforms associated with the shoreline in the study area, a set of shoreline proxies such as the cliff top line or the vegetation line was used to digitize as the shoreline (Figure 2). The only interruption of the shoreline was along the delta of Babbage River, which was excluded because no clear shoreline was distinguishable. The Babbage River delta is approximately 4.2 km wide (linear distance) at its entrance to the Beaufort Sea. If the geomorphological setting changed throughout the years, for example, from an actively eroding to an inactive cliff, the same shoreline proxy was used for all time periods. Thus, even though different proxies were used at different locations, the proxy used at each area was consistent through time. In this case, the shoreline proxy that could be distinguished best in both images was selected. The same approach was used when a shoreline proxy could not be distinguished in an image because of terrain shadows or cloud cover.

Figure 2. Examples of coastal landforms associated with the five coastal landform classes used to describe the shoreline (for definitions, see Table 5). The shoreline proxies used to digitize the shoreline are provided in brackets. The legend applies to all panels.

For computation of shoreline change rates, the position of the shoreline at the beginning was compared to the position of the shoreline at the end of a time step. The uncertainty of each shoreline position (U) was calculated as shown in equation (1):

$$U = \sqrt{\left(E^2_{\text{GR aerial image}} + E^2_{\text{GR satellite image}} + \text{RMS}^2 + \text{LOA}^2 \right)}, \tag{1}$$

where $E_{\text{GR satellite image}}$ is the ground resolution of the satellite images, $E_{\text{GR aerial image}}$ represents the ground resolution of the aerial images from a particular decade, RMS is the root mean square error associated with the geocoding of aerial images from the respective decade, and LOA is the estimated loss of accuracy for the respective decade (Table 2; equation modified after Hapke & Reid, 2007). The LOA accounts for the digitizing error and was determined by calculating the variance associated with repeated shoreline digitization of the same extent of shoreline. For consistency, all shorelines were digitized by the same operator.

Table 3
Dilution of Accuracy (DOA) for All Considered Time Periods

Time period	DOA (m/a)
1950s–1970s	0.8
1970s–1990s	0.6
1990s–2011	0.3
1970s–2011	0.3
1950s–2011	0.2

Note. In order to account for the date mismatch, the DOA calculations were performed with the shortest possible time period which results in the highest DOA.

2.2.3. Calculation of Shoreline Position Change Rates

Shoreline change rates were calculated using the Esri ArcGIS extension Digital Shoreline Analysis System (DSAS) version 4.3 (Thieler et al., 2009). The rates of shoreline change were computed along transects perpendicular to the shoreline, with a transect spacing of 100 m. For each transect and each time step, the mean rates of shoreline change per year (the DSAS output parameter is called end point rate) were calculated. DSAS analyses were conducted for the time step from the 1950s to the 1970s, the 1970s to 2011, and the 1950s to 2011 for the whole study area. For each decade, an average date was calculated from all image acquisition dates and used for DSAS analyses. The date 16 August 1953 was used for the 1950s, 17 July 1972 was used for the 1970s shoreline, and 16 August 2011 for the 2011s shoreline. Additionally, shoreline change rates were calculated for the 1970s to the 1990s and from the 1990s to 2011 for the six areas where shoreline position data from the 1990s was available. In the following sections, these segments of coast that are covered in all image series, including the 1990s, are referred to as key sites. The 1990s images cover a total, but discontinuous, shoreline length of 27 km, which accounts for 13% of the whole shoreline (Figure 1). The actual image acquisition dates were used for DSAS (06 August 1992, 13 July 1994, and 25 July 1996). All computed DSAS shoreline change rates for each transect are published in form of a comma separated value file in PANGAEA (Irrgang et al., 2017).

An indicator for the accuracy of the calculated shoreline change rate is the dilution of accuracy (DOA). The DOA was calculated as is shown in equation (2):

$$\text{DOA} = \frac{\sqrt{U_1^2 + U_2^2}}{\Delta t}, \qquad (2)$$

where U_1 is the uncertainty of the shoreline position from the first point in time, U_2 is the uncertainty of the shoreline position from the second point in time, and Δt is the amount of years covering the analyzed time span (equation modified after Foster & Savage, 1989). In order to account for the date variability for the 1950s and 1970s aerial images, the shortest possible time span (Δt) was chosen for each DOA calculation. This results in highest possible DOA values for each calculation. Table 3 displays the DOAs for all analyzed time periods. The respective DOA is added to each shoreline change rate.

2.2.4. Method for Change Detection Along Lagoons, Barrier Island, and Spits (Gravel Features)

For the purpose of this study, erosion is defined as a landward movement and accretion as a seaward movement of the shoreline. This definition can be misleading if it comes to shoreline dynamics along lagoons, barrier islands, and spits since a landward movement of these geomorphological forms indicates land shift, but not necessarily land loss. In order to capture land loss and land gain more adequately along these features, referred to as gravel features, their areal extent was digitized for the 1950s, 1970s, and 2011 at a scale of 1:1,000. Then, the areas of the generated vector polygon shapefiles were compared. Due to a lack of aerial image coverage, no area calculations could be performed for the 1990s. This analysis was done for the seven largest gravel features that occur along the Yukon coast, namely, Clarence Lagoon, Nunaluk Spit, Catton Point Spit, Stokes Point Lagoon, Kay Point Spit, King Point Lagoon, and Shingle Point Spit. The positions of the gravel features are indicated in Figure 1.

2.3. Field Survey Data

Field site measurements were used to capture local scale coastal changes along 0.3- to 1.7-km-long stretches of coast at subdecadal temporal resolution. For the purpose of this study, data from seven field sites were analyzed for several time periods between 1991 and 2015 (Figure 1, Table 4). The field sites were first established in different years and were surveyed in irregular time steps (Table 4). Multiyear data collection was conducted from 1991 until 1995 using theodolite-based geodetic surveys and since then with the Differential Global Positioning System (DGPS). The theodolite measurements and the DGPS measurements have a position accuracy of ≤5 cm (NRCan, 2013). At all field sites, the DGPS base station was set upon a geodetic benchmark with a known absolute position. At Stokes Point, the geodetic benchmark got lost due to shoreline retreat after 2007, and a new ground control point was established in 2012. Position accuracy of the collected survey information was enhanced by Precise Point Positioning in 2007 and 2012, using the Canadian Spatial

Table 4
Description of the Field Sites

Site name	Survey years	Shoreline length (m)	Number of cross-shore transects
BORs	1991, 1999, 2006, 2012, 2015	120	3
CLAs	1997, 2006, 2015	100	3
KOMs	1997, 2000, 2006, 2012, 2014, 2015	570	9
NUNs	1995, 1996, 1997, 2000, 2003, 2006, 2012, 2014, 2015	100	4
CATs	1996, 2006, 2012, 2014, 2015	420	2
STOs	1995, 1996, 1997, 1999, 2006, 2007, 2012, 2014, 2015,	330	5
KNGs	2012, 2014, 2015	1700	3

Note. Field site positions are shown in Figure 1. Each site is named like the subregion in which it is located with the additional letter s which stands for short, meaning that just a short part of the subregion is covered by GPS measurements. BORs stands for Border$_{short}$ and so on. CLAs is short for Clarence Lagoon, which is situated in the eastern part of the Border subregion. Revisiting of the sites occurred irregularly, with a 1- to 8-year break between two consecutive visits.

Reference System-Precise Point Positioning online tool (NRCan, 2016b). For temporal extension and comparison to remote sensing data, additional transects were created in DSAS that were coincident with the field transects, and separate rate of change statistics were calculated.

2.3.1. Calculation of Shoreline Position Change Rates

Since the field sites were established to serve a variety of purposes (e.g., characterizing representative coastal cliff features, monitoring of archeological sites, and Distant Early Warning line station monitoring), they also have different spatial extents (Table 4). Coastal monitoring was conducted in the form of point measurements along designated cross-shore profiles and along-shore measurements at the water line, at the cliff toe, and at the cliff top. For the calculation of shoreline position change rates, the cliff top was chosen as shoreline proxy. The average annual rate of change (R_{ave}) in meters per year was calculated by dividing the cliff top edge position differences (Δx and Δy) by the number of years in between two consecutive measurements (Δt):

$$R_{ave} = \frac{\sqrt{(\Delta x)^2 + (\Delta y)^2}}{\Delta t} \tag{3}$$

2.4. Classification of Shoreline

To classify the variety and distribution of coastal landforms along the Yukon coast, a coastal classification scheme was established based on Harper et al. (1985) and Couture et al. (2015). This classification scheme was applied to the shoreline from the year 2011 at a scale of 1:1,000. Figure 2 shows examples for each of the five established classes, being (1) beach, barrier island, and spit; (2) inundated tundra; (3) tundra flats; (4) tundra slopes; and (5) active tundra cliff. Table 5 contains the definition of each class.

2.5. Transectwise Analyses of Shoreline Movements Through Time

In order to better understand the evolution of the shoreline between the different time periods, a detailed analysis of the movement of the shoreline at each DSAS transect was performed. Transects were categorized based on whether shoreline change rates showed increasing or decreasing erosion, increasing or decreasing accumulation, whether accumulation changed to erosion, or vice versa. This transectwise analysis was performed to compare two consecutive time periods (1950s–1970s with 1970s-2011), over the whole length of coast and to compare three consecutive time periods (1950s–1970s with 1970s–1990s and 1970s–1990s with 1990s–2011) for the key sites extent.

3. Results

The results provide shoreline change rates along the 210-km length of the Yukon coast for the time between 1951 and 2015 (Figure 3, supporting information Figure S4). The mean rate of shoreline change for the whole length of coast was -0.7 ± 0.2 m/a. Thirteen percent of the coast was either accumulating or stable while 87% of the coast was eroding. All computed DSAS shoreline change rates are published in a comma-separated value file in PANGAEA (Irrgang et al., 2017).

In order to quantify how well the key sites capture the variability of coastal landforms of the whole coast, percentages of the coastal landforms for both extents were compared. Compared to the whole coast, key sites

Table 5
Coastal Landform Classification and Respective Shoreline Proxies

Coastal landform class	Definition	Main shoreline proxy
Beach, barrier island, and spit	Subaerial sand and gravel beaches that are surrounded by water from both sides, such as spit extensions from the mainland, barrier islands fronting the mainland, lagoons, and river inlets	Instantaneous land/water interface
Inundated tundra	Tundra inundated due to thaw subsidence and/or coastal flooding as an effect of sea-level rise. This class includes wetlands and tidal flats	Vegetation line
Tundra flats	Low lying tundra with no evident active cliff or inactive cliff	Vegetation line
Tundra slopes	Inactive cliffs and inactive retrogressive thaw slumps that are flattened and vegetated due to the absence of coastal erosion	Edge of cliff toe
Active tundra cliff	Cliffs and bluffs which are actively eroding	Edge of cliff top

overrepresent the active tundra cliff landform and underrepresent low-lying forms such as beaches, bars, spits, and inundated tundra. The active tundra cliff class contains the most uniformly and rapidly retreating shoreline sections. Its overrepresentation among the key sites results in more negative mean shoreline change rates compared to the whole coast. Consequently, the key sites serve as an indicator for how the more dynamic parts of the coast are changing.

3.1. Temporal Variations in Shoreline Change Rates

Temporal changes in shoreline positions were analyzed for five observation time periods (1950s–1970s, 1970s–2011, 1950s–2011, 1970s–1990s, and 1990s–2011), based on images from the 1950s, 1970s, 1990s, and 2011 (Table 6). Throughout all time periods, the mean shoreline change rate of the whole coast remained stable. The mean rate of shoreline change of -0.7 ± 0.2 m/a varied only marginally over time (1950s–1970s: -0.7 ± 0.8 m/a, 1970s–2011: -0.7 ± 0.3 m/a; Table 6) and did not change significantly (level of significance $\alpha = 0.05$).
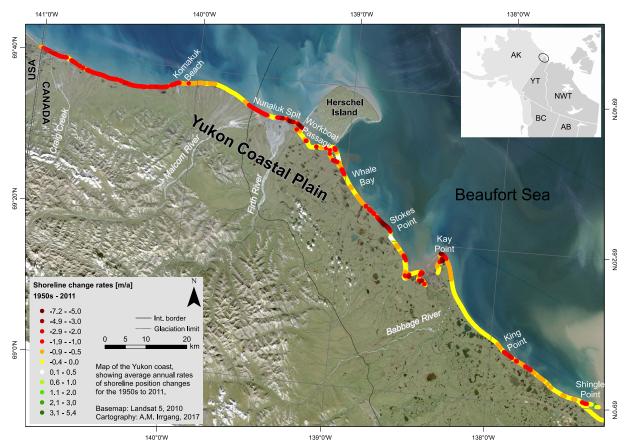

Figure 3. Generalized spatial distribution of mean annual shoreline change rates for the 1950s to 2011 time period. For detailed shoreline change rates, see Figure S4 in the supporting information.

Table 6
Rate of Shoreline Change Statistics for All Analyzed Time Steps for the Whole Study Area and for the Key Sites

Extent	Time period	Mean rate of change (m/a)	Median rate of change (m/a)	ER (% of all measurements)	ER ≤ −1 (% of all measurements)	AC (% of all measurements)	AC ≥ 1 (% of all measurements)
Whole coast	1950s–1970s	−0.7 ± 0.8	−0.5	77	34	23	4
	1970s–2011	−0.7 ± 0.3	−0.5	84	29	16	2
	1950s–2011	−0.7 ± 0.2	−0.5	87	30	13	2
Key sites	1950s–1970s	−1.3 ± 0.8	−1.2	86	53	14	2
	1970s–1990s	−0.5 ± 0.6	−0.6	78	32	22	6
	1990s–2011	−1.3 ± 0.3	−1.2	85	55	15	4
	1970s–2011	−0.9 ± 0.3	−0.9	88	47	12	2
	1950s–2011	−1.0 ± 0.2	−1.0	87	53	13	1

Note. The key sites have additional information because of the use of 1990s aerial images. The 1990s aerial images cover 27 km of the whole study area, and the rate of change statistics were compiled specifically for their spatial extent. ER stands for erosion, and AC stands for accumulation. See supporting information S5 for a separate list of all statistics for each key site.

Along the key sites, after a significant decrease in negative shoreline change rates in the 1970s to 1990s time period in comparison to the 1950s to 1970s time period, a strong acceleration in erosion was measured since the 1990s. A mean rate of shoreline change of −1.3 ± 0.8 m/a was measured for the 1950s to 1970s. In the 1970s to 1990s time period, the mean rate of shoreline change decreased significantly to −0.5 ± 0.6 m/a. The mean rate of shoreline change for the 1990s to 2011 time period (−1.3 ± 0.3 m/a) was not significantly different from the previous time period ($\alpha = 0.05$) but nearly twice as high as the mean rate of shoreline change for the whole coast (−0.7 ± 0.2 m/a). Forty-nine percent of the coast is classified as either inundated tundra or active tundra cliff (Table 8).

Transectwise analyses performed along the whole coast show that the amount of transects recording erosion increased from the 1950s to 1970s time period to the 1970s to 2011 time period from 78% to 84% (Figure 4a). However, along 36% of these transects, shoreline change rates decreased from the 1950s to 1970s time period to the 1970s to 2011 time period (Figure 4a). The amount of transects along which erosion rates of more than −5 m/a were measured increased in the 1970s to 2011 time period (compare amount of pale and dark red dots beyond the −5 m/a mark in Figure 4a).

Transectwise analyses performed at the key sites show a deceleration in erosion from the 1950s to 1970s time period to the 1970s to 1990s time period, followed by a shift back to a more highly erosive regime during the 1990s to 2011 time period. The comparison of rates of shoreline change of the 1950s to 1970s time period with the 1970s to 1990s time period shows that coastal erosion decelerated along 49% of the key sites transects (Figure 4b). Over the same period of time, 15% of the key sites transects shifted from erosion to accumulation. In the following time period, from the 1990s to 2011, a strong acceleration in erosion was measured along 54% of all key site transects (Figure 4c). In summary, the key sites first showed a shift toward a strong decrease in the percentage of eroding transects, which was followed by an increase in the percentage of eroding transects and an acceleration of erosion in the most recent time period, which is in magnitude similar to the earliest time period.

3.2. Alongshore Variations in Shoreline Change Rates

The study area was subdivided into nine subregions to characterize the spatial variability of shoreline changes along the Yukon coast (Table 7, Figures 1 and 5). The subregions' divisions were placed at boundaries between physiographical units. Additionally, it was considered that the coast within each subregion has similar orientation.

Over the 1950s to 2011 time period, the western Yukon coast (west of Herschel Island) experienced more negative mean annual rates of shoreline change than did the eastern Yukon coast. Change occurred at the Border, Komakuk Beach, and Nunaluk Spit subregions at mean shoreline change rates of −1.4 ± 0.2, −1.3 ± 0.2, and − 0.9 ± 0.2 m/a, respectively. With mean shoreline change rates of −0.1 ± 0.2 to −0.5 ± 0.2 m/a, the subregions south and east of Herschel Island were closer to the overall mean rate of shoreline change of −0.7 ± 0.2 m/a along the whole coast.

The highest erosion rates were measured in the Nunaluk Spit (−7.2 ± 0.2 m/a) and Stokes Point (−6.2 ± 0.2 m/a) subregions and were associated with the beach, barrier island, and spit class. In the Kay
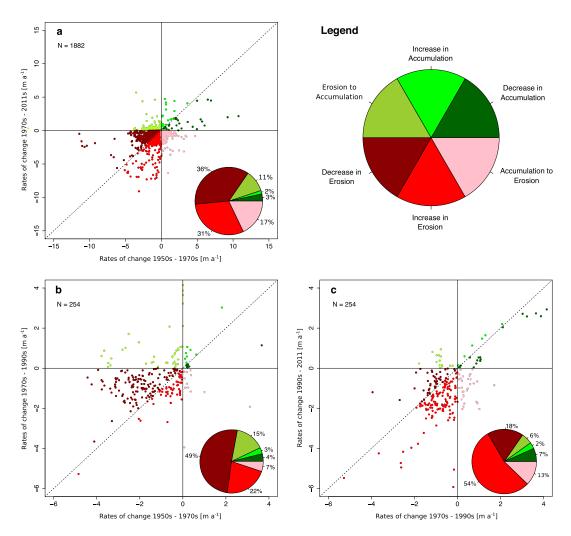
Figure 4. Transectwise analyses of shoreline movements for the whole coast (a) and for the key sites (b, c). Each point in the scatter plot stands for measurements of rates of change along one DSAS transect in two consecutive time periods. The colors in the pie charts correspond to the colors in the graphs.

Table 7
Rate of Shoreline Change Statistics for Coastal Subregions Arranged From West to East (Figure 1) over the 1950s to 2011 Time Period

Subregion	Coverage, km (%)	Max. ER rate (m/a) ± 0.2	Mean rate of change (m/a) ± 0.2	Median rate of change (m/a) ± 0.2	Max. AC rate (m/a) ± 0.2	ER along subregion, % (ER ≤ −1 m/a)	AC along subregion, % (AC ≥ 1 m/a)	ER along coast, % (ER ≤ −1 m/a)	AC along coast, % (AC ≥ 1 m/a)
BOR	11.7 (5.6)	−2.1	−1.4	−1.3	0.0	99.1 (71.8)	0.9 (0.0)	5.5 (4.0)	0.1 (0.0)
KOM	24.5 (11.5)	−2.0	−1.3	−1.3	/	100.0 (77.1)	0.0 (0.0)	11.5 (8.9)	0.0 (0.0)
NUN	29.1 (13.9)	−7.2	−0.9	−1.1	5.0	95.2 (39.9)	4.8 (2.6)	13.2 (5.5)	0.7 (0.4)
WBP	23.2 (11.0)	−2.5	−0.3	−0.4	0.6	86.2 (12.4)	13.8 (0.0)	9.5 (1.4)	1.5 (0.0)
WHB	14.3 (6.8)	−1.5	−0.5	−0.5	0.2	93.3 (13.4)	6.7 (0.0)	6.4 (0.9)	0.5 (0.0)
STO	31.9 (15.2)	−6.2	−0.5	−0.9	2.9	79.9 (31.4)	20.1 (3.0)	12.2 (4.8)	3.1 (0.5)
KAY	33.6 (16.0)	−5.8	−0.2	−0.5	0.9	83.8 (9.5)	16.2 (0.0)	13.4 (1.5)	2.6 (0.0)
KNG	20.6 (9.8)	−2.5	−0.5	−0.6	2.5	95.3 (20.7)	4.7 (1.6)	9.4 (2.0)	0.5 (0.2)
SHI	21.2 (10.1)	−1.8	−0.1	0.1	5.3	63.3 (4.5)	36.7 (8.0)	6.4 (0.5)	3.7 (0.8)

Note. AC stands for accumulation and ER for erosion. See Figure 1 for locations. The values in parentheses in column 2 (coverage) show how many percent of the total shoreline length is covered by the respective subregion. The values in parentheses in the remaining columns indicate how many percent of the shoreline is eroding or accreting with a rate of more than 1 m/a.
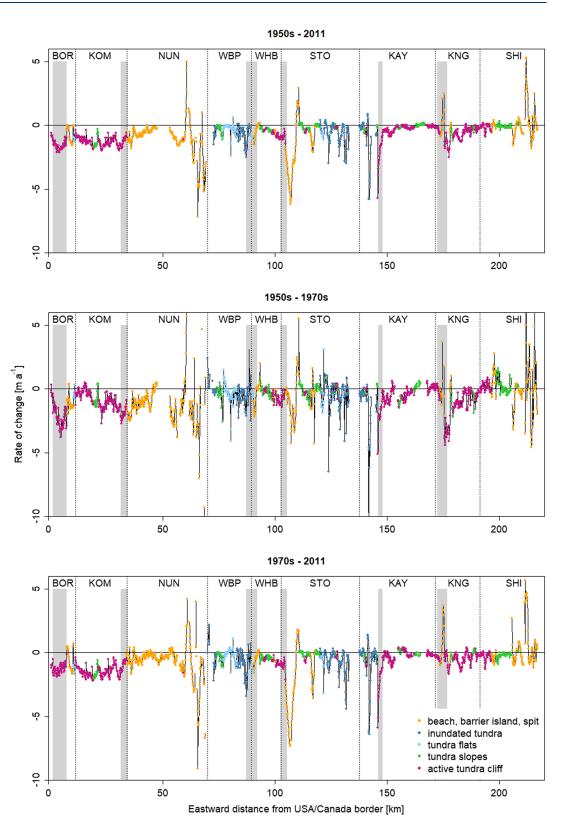
Figure 5. Rates of change for the time period of the 1950s to 2011, 1950s to 1970s, and 1970s to 2011 along the coast with corresponding coastal landform classes (colored dots) and key site extents (gray bars). Negative rates of shoreline change indicate erosion, and positive rates indicate accumulation. See Figure 1 for locations. Gaps in the plot are resulting from missing coverage by aerial imagery in the 1950s (NUN), the missing digitalization of the Babbage River delta (STO), or shoreline aggradation in 2011 due to longshore drift (SHI).

Table 8
Coastal Landform Classes and Corresponding Rate of Shoreline Change Statistics for the 1950s to 2011 Time Period

Class	Coverage, km (%)	Max. ER rate (m/a) ± 0.2	Mean rate of change (m/a) ± 0.2	Median rate of change (m/a) ± 0.2	Max. AC rate (m/a) ± 0.2	ER in class, % (ER ≤ −1 m/a)	AC in class, % (AC ≥ 1 m/a)	ER along coast, % (ER ≤ −1 m/a)	AC along coast, % (AC ≥ 1 m/a)
Beach, barrier island, spit	61.7 (29.4)	−7.2	−0.9	−0.7	5.3	82.4 (36.7)	17.6 (6.1)	24.2 (10.8)	5.2 (1.8)
Tundra slopes	35.2 (16.8)	−1.8	−0.2	−0.1	0.3	75.8 (6.1)	24.2 (0.0)	12.7 (1.0)	4.1 (0.0)
Inundated tundra	23.8 (11.3)	−5.8	−0.8	−0.5	0.9	85.7 (23.8)	14.3 (0.0)	9.7 (2.7)	1.6 (0.0)
Tundra flats	9.9 (4.7)	−2.4	−0.5	−0.4	0.6	95.7 (14.0)	4.3 (0.0)	4.5 (0.7)	0.2 (0.0)
Active tundra cliff	79.3 (37.8)	−5.7	−0.8	−0.8	0.2	96.2 (38.1)	3.8 (0.0)	36.3 (14.4)	1.4 (0.0)
Whole coast	210 (100.0)	−7.2	−0.7	−0.5	5.3			87.5 (30.5)	12.5 (1.9)

Note. AC stands for accumulation and ER for erosion. The values in parentheses in column 2 (coverage) show how many percent of the total shoreline length is covered by the respective landform class. The values in parentheses in the remaining columns indicate how many percent of the shoreline is eroding or accreting with a rate of more than 1 m/a.

Point subregion, very high erosion rates were also measured at −5.8 ± 0.2 and −5.7 ± 0.2 m/a. These were associated with the inundated tundra class in the wave-sheltered area southeast of Kay Point Spit and with the active tundra cliff class at the very tip of King Point. Along 30.5% of all transects, erosion rates higher than −1.0 ± 0.2 m/a were recorded. The subregions of Komakuk Beach, Nunaluk Spit, and Stokes Point had the largest amounts of these high erosion rates, with 8.9%, 5.5%, and 4.8%, respectively. Most of these high erosion rates were associated with the active tundra cliff class (14.4%) and to a lesser extent with the beach, barrier island, and spit class (10.8%). These two classes not only contain the highest rates of erosion but also cover the longest stretches of the coast.

The highest accumulation rates were measured in the Shingle Point (5.3 ± 0.2 m/a), Nunaluk Spit (5.0 ± 0.2 m/a), and Stokes Point (2.9 ± 0.2 m/a) subregions and were associated with the beach, barrier island, and spit class (Figure 3). Along 1.9% of all transects, accumulation rates of more than 1.0 m/a were recorded. The subregions of Shingle Point, Stokes Point, and Nunaluk Spit had the largest amount of these high accumulation rates, with 0.8%, 0.5%, and 0.4%, respectively. Most accumulation rates were associated with the beach, barrier island, and spit class and the tundra slopes class.

In summary, the subregions of Nunaluk Spit and Stokes Point showed the highest spatial variability (i.e., the greatest range) in shoreline change rates, whereas the subregions of Komakuk Beach and Border had the most uniformly changing shorelines, which were only eroding (Table 7, Figure 5). The class of beach, barrier island, and spit showed the highest variability in shoreline change rates, whereas shoreline positions in the tundra slopes class varied the least (Table 8, Figure 5).

3.3. Shoreline Dynamics Along Field Sites

Results derived from the GPS measurements and corresponding DSAS measurements along the field sites (Figure 6) are in good agreement with the analyses of the remotely sensed data. Since 2012, measurements along the field sites Border (BORs), Nunaluk Spit (NUNs), and Stokes Point (STOs) revealed shoreline change rates of −3.3, −2.2, and −8.9 m/a, respectively (Figure 6). These are the highest rates measured since the beginning of the monitoring. In contrast, mean annual rates of shoreline change along Clarence Lagoon (CLAs) and King Point (KNGs) were highest in the 1950s to 1970s time period (CLAs = 2.9 ± 0.2 m/a, KNGs = 4.3 ± 0.2 m/a) and decreased by 96% and 74% since then (CLAs = 0.1 m/a in 2006–2015, KNGs = 1.1 m/a in 2012–2015). Measurements along the Komakuk Beach (KOMs) field site show that shoreline change along this site seems to follow an interannual pattern, where each 10 years the coast erodes faster, followed by a gradual deceleration of erosion (Figure 6). Measurements along Catton Point show that this field site is stable—no change through time was recorded. This site is not included in Figure 6.

Except for the measurements along Clarence Lagoon, Catton Point and King Point, rates of shoreline change measured since 2006 at the field sites were up to 13 times higher than the regional long-term mean of −0.7 ± 0.2 m/a for the 1950s to 2011.

3.4. Dynamics of Lagoons, Barrier Islands, and Spits (Gravel Features)

Six out of seven gravel features analyzed along the Yukon coast expanded in area within the 1950s to 2011 time period (Figure 7). The largest change, with an increase of 110%, was detected along the lagoon at King
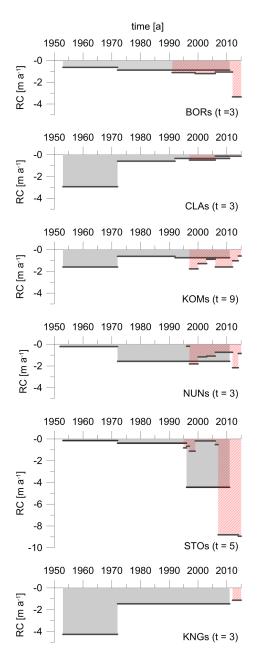
Figure 6. Rates of shoreline change along six out of seven field sites. The field site of Catton Point was neither eroding nor accumulating throughout all time periods and is thus not displayed here. The GPS measurements (red shaded bars) are shown together with the remote sensing measurements (gray bars). RC stands for rate of shoreline change. The t in the brackets indicates the number of transects along the respective field site. The field site positions are indicated in Figure 1. Each site is named like the subregion in which it is located with the additional letter s that stands for short, meaning that just a short part of the subregion is covered by GPS measurements. BORs stands for Border$_{short}$ and so on. CLAs is short for Clarence Lagoon that is situated in the eastern part of the Border subregion. Additional information about the field sites can be obtained from Table 4.

Point. The lagoon closed between the 1950s and the 1970s and since then grew to an extent of approximately 366,200 m^2 in 2011. Since the 1950s, Kay Point Spit, which is situated just north of the rapidly eroding tip of Kay Point, increased in area by half of its size (51%). The largest gravel feature along the Yukon coast is Nunaluk Spit, with a total area of 3,064,500 m^2 in 2011, 39% more than in the 1950s. The two gravel features that show smallest changes since the 1950s are closures of lagoons. In 2011, Stokes Point lagoon was 12% larger than in the 1950s. Clarence Lagoon decreased in size since the 1950s.

3.5. Yukon Territory Land Loss

From the 1950s to 2011, a total area of approximately 8,323,100 m^2 was lost along the coast of the Yukon Territory due to shoreline retreat, which is on average approximately 14 ha/a. However, the definition of coastal erosion and accretion used for this calculation does not adequately capture the full dynamics of gravel features such as barrier islands, spits, and lagoon beaches, which can be sites of sediment deposition and net accumulation despite shifting toward the mainland. The calculation was therefore performed once more, excluding the seven main gravel features (Figure 1). In this case, 5,985,500 m^2 of land were lost along the Yukon coast due to coastal erosion over the 1950s to 2011 period, which is on average approximately 10 ha/a.

4. Discussion

4.1. Temporal Variations in Shoreline Change Rates

Mean shoreline change rates of -0.7 ± 0.2 m/a along the 210 km of the Yukon coast indicate long-term stability of spatially averaged shoreline change rates from the 1950s to 2011 (Table 6). The overall rate is in good agreement with Harper et al. (1985), who calculated a mean annual shoreline change rate of -0.5 m for the time period of the early 1950s to 1970s, but is considerably smaller than the mean shoreline change rate of -1.12 m/a, published by Lantuit et al. (2012) for the Canadian Beaufort coast, which represents the overall mean rate of shoreline change averaged from several data sets, covering time spans since the 1950s to 2000. A potential reason for the higher negative shoreline change rate from Lantuit et al. (2012) is that it comprises rates of shoreline change from the whole Canadian Beaufort coast, including the Mackenzie River delta and its outer islands and up to the northern end of Banks Island. These regions are oriented northwest to west and are therefore directly exposed to the most effective storms, resulting in higher negative mean shoreline change rates (Solomon, 2005).

Three possible explanations for the stability of the mean shoreline change rate through time are that (1) the driving environmental factors did not change for long enough or not by a great enough magnitude for the coastal system to manifest in a change, (2) that changes that were occurring along the coast are averaged out by the overall mean rate of shoreline change, or (3) that the temporal resolution of the shoreline change rates is too low to capture changes in the system. Observations show that environmental factors such as sea surface, water, and air temperatures and the length of the open water season are changing over the past few decades—temperatures are rising and open water seasons are getting longer (Hinzman et al., 2005; Parkinson & Comiso, 2013; Serreze & Barry, 2011; Stroeve et al., 2014). These changes may lead to higher erosion rates along the coast (Barnhart, Overeem, et al., 2014). The average rate of shoreline change was compiled with nearly
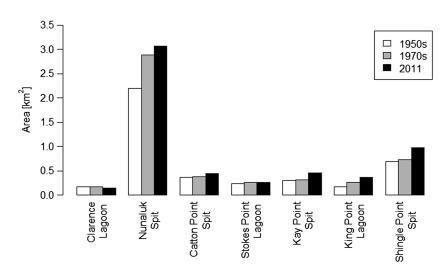
Figure 7. Areas of the seven largest gravel features along the Yukon coast measured in the 1950s, 1970s, and 2011. The areas are displayed from west to east. For positions, see Figure 1.

2,000 measurements along 210 km of coast. This averaging involves an inevitable smoothing of the highly dynamic areas, as can be seen in Figure 5. Yet the number of transects shifting from accumulation in the 1950s to 1970s to erosion in the 1970s to 2011(17%) was over 50% higher than the number of transects shifting from erosion to accumulation (11%; Figure 4a), indicating a change in the erosion versus accumulation regime along the coast. Also, the number of transects recording shoreline retreat rates of more than −5 m was higher in the most recent time period of the 1970s to 2011. Thus, a change toward higher erosion is observed (Figure 4A) but not reflected in the overall mean shoreline change rates (Table 6).

The key sites show a different trend in mean shoreline change rates. The analyses of the key sites included the 1990s images and provided a greater temporal resolution, with three equally long time steps of roughly 20 years (1950s–1970s, 1970s–1990s, and 1990s–2011; Table 6). These analyses suggest that mean shoreline retreat across the key sites decelerated significantly between the 1970s and 1990s, followed by an increase in shoreline retreat from the 1990s to 2011 back to the height of the 1950s to 1970s rates (Table 6). In a similar study, conducted at Herschel Island, a decrease in coastal erosion in between the 1954 to 1970 and the 1970 to 2000 time periods was also observed (Lantuit & Pollard, 2008). One explanation for this large-scale coastal dynamics pattern is a change in storm climatology. An analysis of wind data for study sites east of the Mackenzie Delta and for Kay Point revealed that there was a phase of greater storminess in the early to mid-1960s in comparison to the 1950s, followed by a quieter phase from the late 1960s and most of the 1970s (Manson et al., 2005; Solomon et al., 1994). This period was followed by a renewed phase of enhanced storm activity from the 1980s up to the end of the study in 2000 (Manson et al., 2005; Solomon et al., 1994). A similar analysis of storm reanalysis data for the Yukon coast that would allow linking the variability in rates of shoreline change to varying storm patterns is missing at the present.

The GPS measurements at the field sites extend until 2015 and show that a pattern of increasing negative shoreline change rates with intensifying erosion since 2006 along the sites of BORs, KOMs, and STOs (Figure 6). The observation of an acceleration of coastal erosion since the early 1990s is in good agreement with findings from the Alaskan part of the Beaufort coast and from the Siberian coast (Günther et al., 2013; Jones, Arp, Jorgenson, et al., 2009; Mars & Houseknecht, 2007; Maslakov & Kraev, 2016; Ping et al., 2011). The latest observations of increasing erosion rates might be partly attributable to the fast declining sea-ice extent since the beginning of this millennium, leading to a longer exposure of the shoreline to waves and to more favorable conditions for the development of higher waves because of a longer fetch (Barnhart, Overeem, et al., 2014; Galley et al., 2016; Overeem et al., 2011; Vihma, 2014). Since the GPS derived rates are calculated for subdecadal time steps, the rates of shoreline change are more susceptible to weather extremes. One severe storm event can, for example, lead to an abnormal high annual erosion rate. Thus, rates of shoreline change averaged over short time periods are often higher and more variable than long-term averages (Dallimore et al., 1996; Dolan et al., 1991). The aerial image analyses are averaging 20- to 40-year time periods so that the observed inter-annual variations have a lower influence, since they are smoothed out by time periods with low erosion.

In summary, temporal changes in coastal dynamics along the Yukon coast show an increase in erosion at some locations in recent years, but this is not necessarily reflected in the long-term mean shoreline change rate. These changes are likely to be linked to changes in the length of the open water season and/or the change of storm intensity and frequency. However, additional work is needed to better link shoreline change dynamics to changes of environmental factors.

4.2. Alongshore Variations in Shoreline Change Rates

On the regional scale, the magnitude of shoreline changes along the Yukon coast seems to be dependent on exposure toward most effective storms that originate from the northwest to north (Hudak & Young, 2002; Manson & Solomon, 2007; Solomon et al., 1994). The regions beyond the Buckland glaciation limit west of Herschel Island (BOR, KOM, and NUN) show mean rates of shoreline change of -1.4 ± 0.2 to -0.9 ± 0.2 m/a, while the shoreline in the regions southeast of Herschel Island (WBP, WHB, STO, KAY, KNG, and SHI) is changing at a mean speed of -0.5 ± 0.2 to -0.1 ± 0.2 m/a (Table 7). The orientation of the mainland coast changes from a north to northwest orientation west of Herschel Island, to a northeast to east orientation east of Herschel Island. The gradient in rates of shoreline change between the regions west and east of Herschel Island suggests that shoreline change rates along the Yukon coast are linked to exposure toward storms, since the predominant direction of storms is north to northwest (Hudak & Young, 2002; Manson & Solomon, 2007; Solomon et al., 1994). The regions west of Herschel Island are directly exposed to the most effective storms. Herschel Island shields the regions to its south (WBP) and east (WHB). These findings are in good agreement with those from Solomon (2005), who observed that rates of shoreline change along the eastern Beaufort coast (Mackenzie Delta to Tuktoyaktuk) are strongly influenced by the exposure to northwest wind-driven waves and the resulting high water levels. The second most prominent direction from which storms originate along the Yukon coast is south-east to south-southeast. However, these storms result in negative surges and are thus less erosive (Harper & Penland, 1982; Henry, 1975).

Publications reporting on shoreline dynamics from the Alaskan side of the Beaufort coast show that shoreline change rates west of Herschel Island correspond well with shoreline change rates in eastern Alaska and that a further increase in erosion toward Point Barrow can be observed (Barnhart, Anderson, et al., 2014; Gibbs & Richmond, 2015; Jones, Arp, Beck, et al., 2009; Ping et al., 2011). A further factor that increases the capacity for higher shoreline retreat rates to the west lies in the presence of high ground ice contents in the cliff. A comparison of shoreline change rates and ground ice contents from the Arctic Coastal Dynamics database (Lantuit et al., 2012) shows that the capacity for erosion rises with rising ground ice contents (Barnhart, Overeem, et al., 2014). Since ground ice contents increase from Herschel Islands toward the west (Couture & Pollard, 2017; Couture et al., 2008) and the resulting high capacity of the ground for coastal erosion is exposed toward the most effective storms, this provides a further explanation of why shoreline change rates are increasingly negative toward the west.

In wave-sheltered areas, relative sea-level rise may play an important role for coastal erosion. All areas that are eroding despite being sheltered from waves lay in the inundated tundra class or to a minor extent in the tundra flats class. Bluffs in these classes are very low, usually not exceeding 2 m in height. Consequently, the inundation of coastal tundra might be attributed to relative sea-level rise, as a consequence of thaw settlement in the coastal zone (Wolfe et al., 1998). That thaw settlement can have a major impact on coastal dynamics, as can be observed in the subregion of Stokes Point (Figure 6: STOs). With a mean shoreline change rate of -8.5 m/a, the area immediately northwest of Stokes Point Lagoon is one of the most rapidly retreating areas along the whole Yukon coast. These high rates of erosion are very limited in extent and are likely to be linked with local controls. In this case, ground ice volume is probably controlling coastal evolution. Along the fast retreating cliff, large bodies of massive ice are visible, which get exposed by coastal erosion. During the summers, the massive ice in the cliff face is exposed to solar radiation, leading to fast melting. Harper (1990) already noticed that large parts of the Yukon coasts are rather melting away than eroding away. During the surveys performed at the field site in 2012, 2014, and 2015, waves were notching the ice-rich cliff face despite unstormy weather conditions, even though aerial images from 1996 showed that there was a beach fronting the cliff. This could be an indicator for a local deepening of the nearshore bathymetry. Ground settlement as a consequence of subsea permafrost or massive ice thaw or another mechanism of active submarine erosion might have caused this local deepening of the nearshore bathymetry, as was observed elsewhere along the Beaufort coast (Brown et al., 2003; Héquette & Barnes, 1990). Thus, Stokes Point is an example for how

place-bound factors, in particular, the amount and state of ground ice volume in the coastal zone, can substantially alter coastal dynamics. The strong control of local geomorphology on coastal dynamics along the Yukon coast was already observed by Harper (1990) and Solomon (2005). However, analyses done by Lantuit, Overduin, and Couture (2008) and Lantuit et al. (2012) suggest that ground ice contents are only weakly correlated with coastal retreat rates, though it seems that the strength of the correlation is very dependent on the local setting.

Along the field sites of Clarence Lagoon (CLAs), Border (BORs), Komakuk Beach (KOMs), and King Point (KNGs; Table 7), shoreline change rates seem to be primarily influenced by alongshore sediment supply and corresponding beach buildup. At the field site that is just west of Clarence Lagoon, a comparison of aerial imagery from the 1950s and 1970s with satellite imagery from 2011 and GPS transect profiles shows that this field site has been fronted by a 20- to 50-m-wide beach since the 1970s. Even though such a narrow beach can be easily flooded during storms, it provides effective protection of the cliff from wave erosion during calm weather conditions. Thus, erosion rates decreased significantly since the 1970s. The opposite can be observed along the Border field site since the early 2000s. The cliff was fronted by an approximately 15-m-wide beach during the 1950s and 1970s, which continuously narrowed since the 1970s and was completely gone by the summer of 2015. Therefore, even low-energetic waves now reach the cliff toe. The cliffs along the Border field site are very ice-rich and susceptible to thermo-abrasion. Along the Komakuk Beach field site, erosion seems to vary decadally, where each 10 years the coast erodes faster, followed by a gradual deceleration of erosion. This pattern could be linked to erosion of large quantities of coarse gravel from the Distant Early Warning line airstrip by large storms. Satellite imagery and field observations show that the beach in front of the airstrip, which contains a considerable amount of coarse construction gravel, shields the location for a considerable amount of time before the reservoir of gravel is exhausted and the airstrip gets eroded by large storms again. Shoreline change rates at the King Point field site were significantly influenced by the closure of the King Point lagoon to the west of the cliff field site. The headland east of the lagoon was comparatively unprotected before the closure of the lagoon, which at least partly explains decreasing erosion rates since the 1970s.

Changes in the rates of shoreline change at the field sites are not consistent with changes for the corresponding coastal subregions. Clearly longer coastal subregions integrate a range of variability including erosional and accumulative features. The field sites function to demonstrate how this variability can be reflected at the local scale. Local scale geomorphological factors, such as ice content in the cliff and beach width, determine the response of the coast to forcing whereas larger scale to synoptic factors, such as storm counts and open water season duration, play a determining role for regional scale shoreline change dynamics.

4.3. Dynamics of Lagoons, Barrier Islands, and Spits (Gravel Features)

Along the Yukon coast, the highest rates of shoreline movement were observed along gravel features. The beach, barrier island, and spit class has the highest peak-to-peak variability in rates of shoreline change (-7.2 ± 0.2 to 5.3 ± 0.2 m/a; Figure 5). Coastal heights in this class do not exceed 2 m and can thaw to a depth of over 1.5 m during summers (Owens & Harper, 1977). Thus, the sands, gravels, and cobbles are reworked by waves during the ice-free season, especially during storms and on a daily basis by longshore currents (Harper, 1990). During the sea ice freeze-up and break-up seasons, as observed along Komakuk Beach, beaches are exposed to the processes of ice-push, through ice pile-ups and ice ride-ups. This can essentially alter the beach geomorphology and is a source of sediment (Harper et al., 1985; Héquette & Barnes, 1990; Hume & Schalk, 1964; Kovacs, 1983; Reimnitz et al., 1990).

Six out of seven investigated gravel features have their largest areal extent in the latest measurement from 2011 (Figure 7). The increase in erosion since the 1990s likely increases the availability of material for the expansion of coastal gravel features such as barrier spits and barrier islands. A different process that may lead to areal expansion is increasing wave energy as a result of higher storminess and sea level rise. This increases the capacity for local sediment redistribution and may lead to flattening and broadening of the gravel features. For Nunaluk Spit, another possible source of sediment, as suggested by Harper et al. (1985), is by ice-push. During overflights in the years of 2012, 2014, and 2015, berms most likely formed by ice-push were visible at the beach of Nunaluk Spit, supporting the hypothesis raised by Harper (1990). In contrast, smallest increase or even a decrease in extent of gravel features was measured along the beaches of Stokes Point Lagoon and Clarence Lagoon. In the updrift direction of the longshore drift that is delivering sediments to

Clarence Lagoon, coastal erosion decreased after 1972; thus, less sediments are being delivered. Along Stokes Point, erosion remarkably intensified after 1994. A possible reason for this is the occurrence of high massive ice contents in the cliffs (section 4.2). Erosion of these cliffs only releases small amounts of sediments. Moreover, a deepening of the nearshore seabed as a consequence of subsea permafrost or massive ice thaw, as is suggested to have happened along Stokes Point, would result in an exposure of the beach to higher wave energy. This causes enhanced sediment mobilization in the upper part of the lagoon and deposition in the down drift direction of the lagoon that is observed toward the south and is continuously growing.

The findings suggest that sediment supply along most parts of the Yukon coast increased through time and since the start of the observation period in 1950s is at its highest today. However, in order to get a better understanding of the dynamics of gravel features along the Yukon coast, information about the volume of these features is needed.

5. Conclusions

In this study, shoreline evolution over 64 years (1951–2015) along a 210-km length of the Yukon coast was examined. The following conclusions can be drawn:

1. The mean rate of shoreline change for a 210-km-long section of the Yukon coast for the 1950s to 2011 amounts to −0.7 ± 0.2 m/a. Although the mean rate of shoreline change stayed approximately the same through time, the total number of transects recording erosion increased through time (78% in the 1950s to 1970s time period, to 84% in the 1970s to 2011 time period), indicating a change in the erosion versus accumulation regime along the coast. Key sites indicate that shoreline retreat significantly increased since the 1990s, following a sharp decrease in rates of shoreline change in the 1970s to 1990s time period compared to the 1950s to 1970s time period.
2. Mean rates of shoreline change for a 210-km-long section of the Yukon coast generally decrease eastward, being highest at the Canada-U.S. American border with −1.4 ± 0.2 m/a and lowest along Shingle Point with a mean rate of −0.1 ± 0.2 m/a. One possible mechanism guiding subregional scale coastal change pattern might be coastal exposure to northwest wind-driven waves and the resulting high water levels.
3. The areal extent of six out of seven main gravel features along the Yukon coast is rising since the 1950s. This might be caused by enhanced sediment availability due to intensified coastal erosion or by flattening of these features by more intensive storms. Monitoring of volumetric changes and water turbidity along the coast would enhance the understanding of sediment dynamics and gravel feature evolution.
4. The Yukon Territory mainland (excluding gravel features) is losing on average 10 ha of land each year over the past 60 years due to the process of coastal erosion. With the prognosticated rise of sea level by the end of this century, along with further effects of climate warming, it is likely that the yearly territorial losses will increase in the future.
5. Sixteen percent of the whole coast has been classified as inundated tundra and tundra flats. In both classes, the shore is characterized by low backshore elevations and is thus prone to flooding, which can be caused by further sea-level rise and by severe storms. Monitoring of the process of ground settlement along some of the subsiding terrains and the installation of a tide gauge along the Yukon coast would enhance the understanding of the processes that are leading to the fast disappearance of these regions and would contribute to a better estimation of impacts of a rising sea level along the Yukon coast in the future.

References

Arctic Monitoring and Assessment Programme (2011). *Snow, water, ice and permafrost in the Arctic (SWIPA): Climate change and the cryosphere* (538 pp.). Oslo, Norway: Arctic Monitoring and Assessment Programme.

Aré, F. E. (1988). Thermal abrasion of sea coasts (part I). *Polar Geography and Geology*, *12*(1), 1–86. https://doi.org/10.1080/10889378809377343

Atkinson, D. (2005). Observed storminess patterns and trends in the circum-Arctic coastal regime. *Geo-Marine Letters*, *25*(2–3), 98–109. https://doi.org/10.1007/s00367-004-0191-0

Barnhart, K. R., Anderson, R. S., Overeem, I., Wobus, C., Clow, G. D., & Urban, F. E. (2014). Modeling erosion of ice-rich permafrost bluffs along the Alaskan Beaufort Sea coast. *Journal of Geophysical Research: Earth Surface*, *119*, 1155–1179. https://doi.org/10.1002/2013JF002845

Barnhart, K. R., Overeem, I., & Anderson, R. S. (2014). The effect of changing sea ice on the physical vulnerability of Arctic coasts. *The Cryosphere*, *8*(5), 1777–1799. https://doi.org/10.5194/tc-8-1777-2014

Bouchard, M. (1974). Surficial geology of Herschel Island, Yukon Territory (M.Sc. thesis). Montréal, Canada: University of Montréal.

Brown, J., Jorgenson, M., Smith, O., & Lee, W. (2003). Long-term rates of coastal erosion and carbon input, Elson Lagoon, Barrow, Alaska, *Eighth International Conference on Permafrost*, 21–25, Zurich, Switzerland.

Burn, C. R., & Zhang, Y. (2009). Permafrost and climate change at Herschel Island (Qikiqtaruq), Yukon Territory, Canada. *Journal of Geophysical Research*, 114, F02001. https://doi.org/10.1029/2008JF001087

Callaghan, T. V., Johansson, M., Prowse, T. D., Olsen, M. S., & Reiersen, L.-O. (2011). Arctic cryosphere: Changes and impacts. *Ambio*, 40(S1), 3–5. https://doi.org/10.1007/s13280-011-0210-0

Couture, N., Forbes, D. L., Fraser, P. R., Frobel, D., Jenner, K. A., Manson, G. K., et al. (2015). A coastal information system for the southeastern Beaufort Sea, Yukon and Northwest Territories (Geological Survey of Canada Open File Report 7778, 17 pp). Retrieved from http://geoscan.nrcan.gc.ca/starweb/geoscan/servlet.starweb

Couture, N. J. (2010). Fluxes of soil organic carbon from eroding permafrost coasts, Canadian Beaufort Sea (PhD thesis). Montréal, Canada: McGill University. Retrieved from http%3A%2F%2Fdigitool.library.mcgill.ca%2FR%2F-%3Ffunc%3Ddbin-jump-full%26amp%3Bobject_id%3D92229%26amp%3Bsilo_library%3DGEN01

Couture, N. J., Hoque, Md. A., & Pollard, W. H. (2008). Modeling the erosion of ice-rich deposits along the Yukon Coastal Plain. In *Conference Proceedings to the Ninth International Conference of Permafrost*. University of Alaska Fairbanks.

Couture, N. J., & Pollard, W. H. (2017). A model for quantifying ground-ice volume, Yukon coast, western Arctic Canada. *Permafrost and Periglacial Processes*, 28(3), 534–542. https://doi.org/10.1002/ppp.1952

Dallimore, S. R., Wolfe, S., & Solomon, S. M. (1996). Influence of ground ice and permafrost on coastal evolution, Richards Island, Beaufort Sea coast, N.W.T. *Canadian Journal of Earth Sciences*, 33(5), 664–675. https://doi.org/10.1139/e96-050

Digital Globe (2014). GeoEye-1 data sheet. Retrieved from https://dg-cms-uploads-production.s3.amazonaws.com/uploads/document/file/97/DG_GeoEye1.pdf

Digital Globe (2016). WorldView-2 data sheet. Retrieved from https://dg-cms-uploads-production.s3.amazonaws.com/uploads/document/file/98/WorldView2-DS-WV2-rev2.pdf

Dolan, R., Fenster, M. S., & Holme, S. J. (1991). Temporal analysis of shoreline recession and accretion. *Journal of Coastal Research*, 7(3), 723–744.

Environment Canada (2016). Historical climate data. Retrieved from http://climate. weather.gc.ca, (last access 15.08.2016).

Environment Yukon (2016). 30 m Yukon digital elevation model. Retrieved from http://www.env.gov.yk.ca/publications-maps/geomatics/data/30m_dem.php, (last access: 18.09.2016).

Forbes, D. L. (1997). Coastal erosion and nearshore variability in the southern Beaufort Sea, Ivvavik National Park, Yukon Territory (Geological Survey of Canada Open File Report 3531).

Forbes, D. L. (Ed.) (2011). State of the Arctic coast 2010—Scientific review and outlook. International Arctic Science Committee, Arctic Monitoring and Assessment Programme, International Polar Association, Helmholtz-Zentrum, 168 Pp, Geesthacht, Germany. Retrieved from http://www.futureearthcoasts.org/state-of-the-arctic-coast-2010-scientific-review-and-outlook/

Foster, E. R., & Savage, R. J. (1989). Methods of historical shoreline analysis. *Coastal Zone*, 89, 4434–4448.

Fritz, M., Lantuit, H., & Vonk, J. (2017). Collapsing Arctic coastlines. *Nature Climate Change*, 7(1), 6–7. https://doi.org/10.1038/nclimate3188

Fritz, M., Wetterich, S., Schirrmeister, L., Meyer, H., Lantuit, H., Preusser, F., & Pollard, W. H. (2012). Eastern Beringia and beyond: Late Wisconsinan and Holocene landscape dynamics along the Yukon Coastal Plain, Canada. *Palaeogeography Palaeoclimatology Palaeoecology*, 319-320, 28–45. https://doi.org/10.1016/j.palaeo.2011.12.015

Galley, R. J., Babb, D., Ogi, M., Else, B. G. T., Geilfus, N. X., Crabeck, O., et al. (2016). Replacement of multiyear sea ice and changes in the open water season duration in the Beaufort Sea since 2004. *Journal of Geophysical Research: Oceans*, 121, 1806–1823. https://doi.org/10.1002/2015JC011583

Gibbs, A. E., & Richmond, B. M. (2015). National assessment of shoreline change—Historical shoreline change along the north coast of Alaska, U.S.-Canadian Border to Icy Cape (U.S. Geological Survey Open File Report 2015–1048, 96 pp.). Retrieved from https://pubs.usgs.gov/of/2015/1030/

Grosse, G., Goetz, S., McGuire, A. D., Romanovsky, V. E., & Schuur, E. A. G. (2016). Changing permafrost in a warming world and feedbacks to the Earth system. *Environmental Research Letters*, 11(4), 40201. https://doi.org/10.1088/1748-9326/11/4/040201

Günther, F., Overduin, P. P., Sandakov, A. V., Grosse, G., & Grigoriev, M. N. (2013). Short- and long-term thermo-erosion of ice-rich permafrost coasts in the Laptev Sea region. *Biogeosciences*, 10(6), 4297–4318. https://doi.org/10.5194/bg-10-4297-2013

Günther, F., Overduin, P. P., Yakshina, I. A., Opel, T., Baranskaya, A. V., & Grigoriev, M. N. (2015). Observing Muostakh disappear: Permafrost thaw subsidence and erosion of a ground-ice-rich island in response to arctic summer warming and sea ice reduction. *The Cryosphere*, 9(1), 151–178. https://doi.org/10.5194/tc-9-151-2015

Hapke, C. J., & Reid, D. (2007). National assessment of shoreline change, part 4: Historical coastal cliff retreat along the California coast. U.S (Geological Survey Open File Report 2007-1133, 51 pp.). Retrieved from https://pubs.usgs.gov/of/2007/1133/

Harper, J. R. (1990). Morphology of the Canadian Beaufort Sea coast. *Marine Geology*, 91(1-2), 75–91. https://doi.org/10.1016/0025-3227(90)90134-6

Harper, J. R., Henry, R. F., & Stewart, G. G. (1988). Maximum storm surge elevations in the Tuktoyaktuk Region of the Canadian Beaufort Sea. *Arctic*, 1(1), 48–52. https://doi.org/10.14430/arctic1691

Harper, J. R., & Penland, P. S. (1982). Beaufort Sea sediment dynamics, Technical report of Woodward-Clyde Consult for Geological Survey of Canada (125 pp.) Victoria, Canada.

Harper, J. R., Reimer, P. D., & Collins, A. D. (1985). Canadian Beaufort Sea physical shore-zone analysis, Report for Northern Oil and Gas Action Plan, Indian and Northern Affairs Canada Ottawa, Canada (105 pp.). Retrieved from http://engineerradcc.library.link/portal/Canadian-Beaufort-Sea-physical-shore-zone/Gu3YaBSD3Pk/

Harris, S.A., French, H. M., Heginbottom, J. A., Johnston, G. H., Ladanyi, B., Sego, D. C., & van Everdingen, R. O. (1988). Glossary of permafrost and related ground-ice terms. National Research Council Canada (Technical Memorandum No. 142, 156 pp.). Retrieved from https://ipa.arcticportal.org/images/Glossary/Glossary_of_Permafrost_and_Related_Ground-Ice_Terms_1998.pdf

Harry, D. G., French, H. M., & Pollard, W. H. (1988). Massive ground ice and ice-cored terrain near Sabine Point, Yukon Coastal Plain. *Canadian Journal of Earth Sciences*, 25(11), 1846–1856. https://doi.org/10.1139/e88-174

Henry, R. F. (1975). Storm surges, Beaufort Sea project (Beaufort Sea Technical Report No. 19, 41 pp.).

Héquette, A., & Barnes, P. W. (1990). Coastal retreat and shoreface profile variations in the Canadian Beaufort Sea. *Marine Geology*, 91(1–2), 113–132. https://doi.org/10.1016/0025-3227(90)90136-8

Héquette, A., Ruz, M.-H., & Hill, P. R. (1995). The effects of the Holocene sea-level rise on the evolution of the southeastern coast of the Canadian Beaufort Sea. *Journal of Coastal Research*, 11(2), 494–507.

Hill, P. R., Blasco, S. M., Harper, J. R., & Fissel, D. B. (1991). Sedimentation on the Canadian Beaufort shelf. *Continental Shelf Research*, 11(8–10), 821–842. https://doi.org/10.1016/0278-4343(91)90081-G

Hinzman, L. D., Bettez, N. D., Bolton, W. R., Chapin, F. S., Dyurgerov, M. B., Fastie, C. L., et al. (2005). Evidence and implications of recent climate change in northern Alaska and other Arctic regions. *Climatic Change*, *72*(3), 251–298. https://doi.org/10.1007/s10584-005-5352-2

Huber, M., Gruber, A., Wendleder, A., Wessel, B., Roth, A., & Schmitt, A. (2012). The global TanDEM-X DEM: Production status and first validation results. *The International Archives of the Photogrammetry, Remote Sensing and Spatial Information Sciences*, *XXXIX-B7*, 45–50. https://doi.org/10.5194/isprsarchives-XXXIX-B7-45-2012

Hudak, D. R., & Young, J. M. C. (2002). Storm climatology of the southern Beaufort Sea. *Atmosphere-Ocean*, *40*(2), 145–158. https://doi.org/10.3137/ao.400205

Hugelius, G., Tarnocai, C., Broll, G., Canadell, J. G., Kuhry, P., & Swanson, D. K. (2013). The northern circumpolar soil carbon database: Spatially distributed datasets of soil coverage and soil carbon storage in the northern permafrost regions. *Earth System Science Data*, *5*(1), 3–13. https://doi.org/10.5194/essd-5-3-2013

Hume, J. D., & Schalk, M. (1964). The effects of ice push on Arctic beaches. *American Journal of Science*, *262*(2), 267–273. https://doi.org/10.2475/ajs.262.2.267

Intergovernmental Panel on Climate Change (2013). Climate change 2013: The physical science basis. In T. F. Stocker et al. (Eds.), *Contribution of Working Group I to the Fifth Assessment Report of the IPCC* (1535 pp.). Cambridge, UK: Cambridge University Press.

Irrgang, A. M., Lantuit, H., Manson, G., Günther, F., Grosse, G., & Overduin, P. P. (2017). Quantification of shoreline movements along the Yukon territory mainland coast between 1951 and 2011. Dataset #874343. https://doi.org/10.1594/PANGAEA.874343

James, T. S., Henton, J. A., Leonard, L. J., Darlington, A., Forbes, D. L., & Craymer, M. (2014). Relative sea-level projections in Canada and the adjacent mainland United States; Geological Survey of Canada, Ottawa, Ontario (Open File 7737, 72 pp.). Retrieved from http://ftp2.cits.rncan.gc.ca/pub/geott/ess_pubs/295/295574/of_7737.pdf

Jones, B. M., Arp, C. D., Beck, R. A., Grosse, G., Webster, J. M., & Urban, F. E. (2009). Erosional history of Cape Halkett and contemporary monitoring of bluff retreat, Beaufort Sea coast, Alaska. *Polar Geography*, *32*(3–4), 129–142. https://doi.org/10.1080/10889370903486449

Jones, B. M., Arp, C. D., Jorgenson, M. T., Hinkel, K. M., Schmutz, J. A., & Flint, P. L. (2009). Increase in the rate and uniformity of coastline erosion in Arctic Alaska. *Geophysical Research Letters*, *36*, L03503. https://doi.org/10.1029/2008GL036205

Jones, B. M., Hinkel, K. M., Arp, C. D., & Eisner, W. R. (2008). Modern erosion rates and loss of coastal features and sites, Beaufort Sea coastline, Alaska. *Arctic*, *61*(4), 361–372. https://doi.org/10.14430/arctic44

Jones, B. M., Stoker, J. M., Gibbs, A. E., Grosse, G., Romanovsky, V. E., Douglas, T. A., et al. (2013). Quantifying landscape change in an arctic coastal lowland using repeat airborne LiDAR. *Environmental Research Letters*, *8*(4), 45,025–45,010. https://doi.org/10.1088/1748-9326/8/4/045025

Kizyakov, A. I., Zimin, M. V., Leibman, M. O., & Pravikova, N. V. (2013). Monitoring of the rate of thermal denudation and thermal abrasion on the western coast of Kolguev Island, using high resolution satellite images. *Earth cryoshpere*, *17*(4), 36–47.

Kohnert, K., Serafimovich, A., Hartmann, J., & Sachs, T. (2014). Airborne measurements of methane fluxes in Alaskan and Canadian tundra with the research aircraft Polar 5, Reports on Polar and Marine Research (673) (76 pp.). Bremerhaven: Alfred Wegener Institute, hdl:10013/epic.43357.d001

Konopczak, A. M., Manson, G. K., & Couture, N. J. (2014). Variability of coastal change along the western Yukon coast (Geological Survey of Canada Open File Rep. 7516, 61 pp.). Retrieved from http%3A%2F2Fgeoscan.nrcan.gc.ca%2Fstarweb%2Fgeoscan%2Fservlet.starweb%3Fpath%3Dgeoscan%2Fshorte.web%26amp%3Bsearch1%3D293788

Kovacs, A. (1983). Shore ice ride-up and pile-up features. Part II: Alaska's Beaufort Sea coast, U.S. Army Corps of Engineers (51 pp.). Hanover.

Lantuit, H., Atkinson, D., Overduin, P. P., Grigoriev, M., Rachold, V., Grosse, G., & Hubberten, H.-W. (2011). Coastal erosion dynamics on the permafrost-dominated Bykovsky Peninsula, north Siberia, 1951–2006. *Polar Research*, *30*(1), 7341. https://doi.org/10.3402/polar.v30i0.7341

Lantuit, H., Overduin, P. P., & Couture, N. (2008). Sensitivity of coastal erosion to ground ice contents: An Arctic-wide study based on the ACD classification of Arctic coasts. In *Ninth International Conference on Permafrost* (4 pp.). Fairbanks.

Lantuit, H., Overduin, P. P., Couture, N., Wetterich, S., Aré, F., Atkinson, D., et al. (2012). The Arctic coastal dynamics database: A new classification scheme and statistics on Arctic permafrost coastlines. *Estuaries and Coasts*, *35*(2), 383–400. https://doi.org/10.1007/s12237-010-9362-6

Lantuit, H., & Pollard, W. H. (2008). Fifty years of coastal erosion and retrogressive thaw slump activity on Herschel Island, southern Beaufort Sea, Yukon Territory, Canada. *Geomorphology*, *95*(1-2), 84–102. https://doi.org/10.1016/j.geomorph.2006.07.040

Manson, G. K., & Solomon, S. M. (2007). Past and future forcing of Beaufort Sea coastal change. *Atmosphere-Ocean*, *45*(2), 107–122. https://doi.org/10.3137/ao.450204

Manson, G. K., Solomon, S. M., Forbes, D. L., Atkinson, D. E., & Craymer, M. (2005). Spatial variability of factors influencing coastal change in the western Canadian Arctic. *Geo-Marine Letters*, *25*(2–3), 138–145. https://doi.org/10.1007/s00367-004-0195-9

Markus, T., Stroeve, J. C., & Miller, J. (2009). Recent changes in Arctic Sea ice melt onset, freezeup, and melt season length. *Journal of Geophysical Research*, *114*, C12024. https://doi.org/10.1029/2009JC005436

Mars, J. C., & Houseknecht, D. W. (2007). Quantitative remote sensing study indicates doubling of coastal erosion rate in past 50 yr along a segment of the Arctic coast of Alaska. *Geology*, *35*(7), 583–586. https://doi.org/10.1130/G23672A.1

Maslakov, A., & Kraev, G. (2016). Erodibility of permafrost exposures in the coasts of eastern Chukotka. *Polar Science*, *10*(3), 374–381. https://doi.org/10.1016/j.polar.2016.04.009

McDonald, B. C., & Lewis, C. P. (1973). Geomorphic and sedimentologic processes of rivers and coasts, Yukon Coastal Plain. Environ.-Soc. Comm. Northern Pipelines Task Force on Northern Oil Dev. (Rep. 73–79, 245 pp.).

McGuire, A. D., Melillo, J. M., Kicklighter, D. W., & Joyce, L. A. (1995). Equilibrium responses of soil carbon to climate change: Empirical and process-based estimates. *Journal of Biogeography*, *22*(4/5), 785–796. https://doi.org/10.2307/2845980

Natural Resources Canada (NRCan) (2013). Guidelines for RTK/RTN GNSS surveying in Canada. Retrieved from http://publications.gc.ca/site/eng/9.822881/publication.html

Natural Resources Canada (NRCan) (2016a). National air photo library. Retrieved from http://www.nrcan.gc.ca/earth-sciences/geomatics/satellite-imagery-air-photos/9265, (last access: 18.09.2016).

Natural Resources Canada (NRCan) (2016b). Canadian Spatial Reference System–Precise Point Positioning (CSRS-PPP). Retrieved from http://www.nrcan.gc.ca/earth-sciences/geomatics/geodetic-reference-systems/tools-applications/10925#ppp, (accessed: 11.03.2017).

Obu, J., Lantuit, H., Fritz, M., Grosse, G., Günther, F., Sachs, T., & Helm, V. (2016). LiDAR elevation data of Yukon Coast and Herschel Island in 2012 and 2013. doi:10.1594/PANGAEA.859046, Supplement to: Obu, J et al. (2016), Dynamics of permafrost coasts along the Canadian Beaufort Sea based on annual airborne LiDAR elevation data. *Geomorphology*. https://doi.org/10.1594/PANGAEA.859046

Obu, J., Lantuit, H., Grosse, G., Günther, F., Sachs, T., Helm, V., & Fritz, M. (2017). Coastal erosion and mass wasting along the Canadian Beaufort Sea based on annual airborne LiDAR elevation data. *Geomorphology*, *293*, 331–346. https://doi.org/10.1016/j.geomorph.2016.02.014

Ogorodov, S. A., Baranskaya, A. V., Belova, N. G., Kamalov, A. M., Kuznetsov, D. E., Overduin, P. P., et al. (2016). Coastal dynamics of the Pechora and Kara Seas under changing climatic conditions and human disturbances. *Geography, Environment, Sustainability*, *9*(3), 53–73. https://doi.org/10.15356/2071-9388

O'Rourke, M. J. E. (2017). Archaeological Site Vulnerability Modelling: The Influence of High Impact Storm Events on Models of Shoreline Erosion in the Western Canadian Arctic. *Open Archaeology*, *3*(1), 1–16. https://doi.org/10.1515/opar-2017-0001

Overduin, P. P., Strzelecki, M. C., Grigoriev, M. N., Couture, N., Lantuit, H., St-Hilaire-Gravel, D., et al. (2014). Coastal changes in the Arctic. In I. P. Martini, & H. R. Wanless (Eds.), *Sedimentary coastal zones from high to low latitudes: Similarities and differences*, *Special Publications. Geological Society of London, Special Publications, 388*, 103–129.

Overeem, I., Anderson, R. S., Wobus, C. W., Clow, G. D., Urban, F. E., & Matell, N. (2011). Sea ice loss enhances wave action at the Arctic coast. *Geophysical Research Letters*, *38*, L17503. https://doi.org/10.1029/2011GL048681

Overland, J., Francis, J. A., Hall, R., Hanna, E., Kim, S. J., & Vihma, T. (2015). The melting arctic and midlatitude weather patterns: Are they connected? *Journal of Climate*, *28*(20), 7917–7932. https://doi.org/10.1175/JCLI-D-14-00822.1

Owens, E. H., & Harper, J. R. (1977). Frost-table and thaw depths in the littoral zone near Peard Bay, Alaska. *Arctic*, *30*(3), 155–168.

Parkinson, C. L., & Comiso, J. C. (2013). On the 2012 record low Arctic Sea ice cover: Combined impact of preconditioning and an August storm. *Geophysical Research Letters*, *40*, 1356–1361. https://doi.org/10.1002/grl.50349

Ping, C.-L., Michaelson, G. J., Guo, L., Jorgenson, M. T., Kanevskiy, M., Shur, Y., et al. (2011). Soil carbon and material fluxes across the eroding Alaska Beaufort Sea coastline. *Journal of Geophysical Research*, *116*, G02004. https://doi.org/10.1029/2010JG001588

Proshutinsky, A., Dukhovskoy, D., Timmermans, M., Krishfield, R., & Bamber, J. L. (2015). Arctic circulation regimes. *Philosophical Transactions of the Royal Society A*, *373*(20140160), 1–18.

Radosavljevic, B., Lantuit, H., Pollard, W., Overduin, P., Couture, N., Sachs, T., et al. (2015). Erosion and flooding—Threats to coastal infrastructure in the Arctic: A case study from Herschel Island, Yukon Territory, Canada. *Estuaries and Coasts*, *39*(4), 900–915. https://doi.org/10.1007/s12237-015-0046-0

Rampton, V. N. (1982). Quaternary geology of the Yukon coastal plain (Geological Survey of Canada, Bulletin 317, 49 pp.). Retrieved from http%3A%2F%2Fgeoscan.nrcan.gc.ca%2Fstarweb%2Fgeoscan%2Fservlet.starweb%3Fpath%3Dgeoscan%2Fshorte.web%26amp%3Bsearch1%3DR%3D111347

Reimnitz, E., Barnes, P. W., & Harper, J. R. (1990). A review of beach nourishment from ice transport of shoreface materials, Beaufort Sea, Alaska. *Journal of Coastal Research*, *6*(2), 439–469.

Reimnitz, E., Graves, S. M., & Barnes, P. W. (1985). Beaufort Sea coastal erosion, shoreline evolution and sediment flux (U.S. Geological Survey Open File Report 85-380).

Reimnitz, E., & Maurer, D. K. (1979). Effects of storm surges on the Beaufort Sea coast, Northern Alaska. *Arctic*, *32*(4), 329–344. https://doi.org/10.14430/arctic2631

Richter-Menge, J., & Mathis, J. (2016). The Arctic [in "State of the Climate in 2015"]. *Bulletin of the American Meteorological Society*, *97*(8), S131–S152.

Serreze, M. C., Barrett, A. P., Stroeve, J. C., Kindig, D. N., & Holland, M. M. (2009). The emergence of surface-based Arctic amplification. *The Cryosphere*, *3*(1), 11–19. https://doi.org/10.5194/tc-3-11-2009

Serreze, M. C., & Barry, R. G. (2011). Processes and impacts of Arctic amplification: A research synthesis. *Global and Planetary Change*, *77*(1–2), 85–96. https://doi.org/10.1016/j.gloplacha.2011.03.004

Smith, S. L., Romanovsky, V. E., Lewkowicz, A. G., Burn, C. R., Allard, M., Clow, G. D., et al. (2010). Thermal state of permafrost in North America: A contribution to the International Polar Year. *Permafrost and Periglacial Processes*, *21*(2), 117–135. https://doi.org/10.1002/ppp.690

Solomon, S. M. (2005). Spatial and temporal variability of shoreline change in the Beaufort-Mackenzie region, northwest territories, Canada. *Geo-Marine Letters*, *25*(2–3), 127–137. https://doi.org/10.1007/s00367-004-0194-x

Solomon, S. M., Forbes, D. L., & Kierstead, B. (1994). Coastal impacts of climate change: Beaufort Sea erosion study (Geological Survey of Canada Open File 2890, 35 pp). Retrieved from http%3A%2F%2Fgeoscan.nrcan.gc.ca%2Fstarweb%2Fgeoscan%2Fservlet.starweb%3Fpath%3Dgeoscan%2Fshorte.web%26amp%3Bsearch1%3DR%3D194148

Stroeve, J., Holland, M. M., Meier, W., Scambos, T., & Serreze, M. (2007). Arctic sea ice decline: Faster than forecast. *Geophysical Research Letters*, *34*, L09501. https://doi.org/10.1029/2007GL029703

Stroeve, J. C., Markus, T., Boisvert, L., Miller, J., & Barrett, A. (2014). Changes in Arctic melt season and implications for sea ice loss. *Geophysical Research Letters*, *41*, 1216–1225. https://doi.org/10.1002/2013GL058951

Stroeve, J. C., Serreze, M. C., Holland, M. M., Kay, J. E., Malanik, J., & Barrett, A. P. (2011). The Arctic's rapidly shrinking sea ice cover: A research synthesis. *Climatic Change*, *110*(3–4), 1005–1027. https://doi.org/10.1007/s10584-011-0101-1

Tanski, G., Lantuit, H., Ruttor, S., Knoblauch, C., Radosavljevic, B., Strauss, J., et al. (2017). Transformation of terrestrial organic matter along thermokarst-affected permafrost coasts in the Arctic. *Science of the Total Environment*, *581-582*, 434–447. https://doi.org/10.1016/j.scitotenv.2016.12.152

Thieler, E. R., Himmelstoss, E. A., Zichichi, J. L., & Ayhan, E. (2009). Digital Shoreline Analysis System (DSAS) version 4.0—An ArcGIS extension for calculating shoreline change (U.S. Geological Survey Open-File Rep. 2008–1278, 79 pp). Retrieved from https://woodshole.er.usgs.gov/project-pages/DSAS/version4/

Thompson, F. (1994). An interpretive manual for reports on granular deposits in the Inuvialuit Settlement Region, Indian and Northern Affairs Canada, Part of the Inuvialuit Final Agreement Implementation Program Task 7 - Sand and Gravel (70 pp.).

Tweedie, C. E., Aguirre, A., Cody, R., Vargas, S., & Brown, J. (2012). Spatial and temporal dynamics of erosion along the Elson Lagoon Coastline near Barrow, Alaska (2002–2011). In *Proceedings of the Tenth International Conference on Permafrost, Volume 1: International Contribution* (pp. 405–430).

Vasiliev, A., Kanevskiy, M., Cherkashov, G., & Vanshtein, B. (2005). Coastal dynamics at the Barents and Kara Sea key sites. *Geo-Marine Letters*, *25*(2–3), 110–120. https://doi.org/10.1007/s00367-004-0192-z

Vihma, T. (2014). Effects of Arctic sea ice decline on weather and climate: A review. *Surveys in Geophysics*, *35*(5), 1175–1214. https://doi.org/10.1007/s10712-014-9284-0.

Vonk, J. E., Sánchez-García, L., van Dongen, B. E., Alling, V., Kosmach, D., Charkin, A., et al. (2012). Activation of old carbon by erosion of coastal and subsea permafrost in Arctic Siberia. *Nature*, *489*(7414), 137–140. https://doi.org/10.1038/nature11392

Wolfe, S. A., Dallimore, S. R., & Solomon, S. M. (1998). Coastal permafrost investigations along a rapidly eroding shoreline, Tuktoyuktut, N.W.T. PERMAFROST—Seventh International Conference (Proceedings) (pp. 1125–1131). Yellowknife.

Wolfe, S. A., Kotler, E., & Dallimore, S. R. (2001). Surficial characteristics and the distribution of thaw landforms (1970 to 1999), Shingle Point to Kay Point, Yukon Territory (Geological Survey of Canada Open File 4115, 18 pp). Retrieved from http%3A%2F%2Fgeoscan.nrcan.gc.ca%2Fstarweb%2Fgeoscan%2Fservlet.starweb%3Fpath%3Dgeoscan%2Fshorte.web%26amp%3Bsearch1%3DR%3D212842

Yukon Department of Environment (2016). 30 meter yukon digital elevation model. Retrieved from http://www.env.gov.yk.ca/publicationsmaps/geomatics/data/30m_dem.php

Zhang, Y., & Chen, W. (2005). Soil temperature in Canada during the twentieth century: Complex responses to atmospheric climate change. *Journal of Geophysical Research*, *110*, D03112. https://doi.org/10.1029/2004JD004910